Automated Hammering Inspection System With Multi-Copter Type Mobile Robot for Concrete Structures

Yuki Nishimura, Shuki Takahashi, Hiromi Mochiyama, and Tomoyuki Yamaguchi

***Abstract*—For infrastructure health monitoring, defects in concrete are periodically inspected by hammering test. Conventional hammering inspection is manually conducted to detect internal concrete defects by recognizing the sounds generated from the hammer strike. Therefore, a robot-based hammering inspection system can realize the inspection automatically. However, those robots have several elements such as noise-resistant acoustic analysis, weight reduction of the robot, constant striking mechanism, and stable robot movement; so integrated research has not been achieved. This paper introduces a hammering inspection system using robot that solves these problems. In the proposed system, a multi-copter type mobile robot realizes a stable attitude on a structure using thrust force to press the robot body onto the structure surface, while a lightweight hammering mechanism constantly strikes a wall. During inspection, noises from multi-copter affect acoustic analysis. Therefore, the proposed method clarifies the features of hammering sound and propeller noise and analyzes hammering sounds. This developed hammering inspection system is the first to realize all functions required for comprehensive hammering inspection, and its accuracy to detect concrete defects from hammering sounds was 81.7% through the experiments.**

***Index Terms*—Hammering test, robot inspection, mobile robot, concrete structures.**

I. Introduction

HAMMERING tests are a contact inspection method for infrastructure. To maintain infrastructure health, periodic inspection is necessary to detect defects in concrete structures. During a periodic inspection, not only surface defects but also internal concrete defects, such as peeling, delamination, and shallows, should be identified. A hammering test, also known as a tapping or impact test, is conducted by manually striking the concrete surface with hammer, while an inspector detects defects by recognizing the sounds generated from the hammer strike. This is a common assessment method for detecting voids from changes in sound [1]. This type of inspection is used to perform a detailed diagnosis of the material condition [2]. However, the number of concrete structures, such as bridges and tunnels, is increasing, and there is an insufficient number of inspectors. Also, there are significant time and monetary costs involved in building scaffolds for inspectors. Therefore, there is a need to automate the hammering test procedure to efficiently carry out concrete structure inspections. In the field of automated inspection, crack detection methods [3] are usually combined with mobile robots [4]–[6] or Unmanned Aerial Vehicles (UAVs) [7], [8] to realize automated inspection. However, unlike vision-based inspection systems, there are relatively few studies on the implementation of automated hammering test systems using robots. To effectively realize hammering inspection using robots, the system requires a hammering device, a mobile robot which can travel on the structure, and an acoustic-based defect classifier for hammering sounds. In this study, an automated hammering inspection robot system is proposed, with a hammering mechanism, acoustic analysis, and a sound and image data recording function, for defect location on concrete structures, as shown in Fig. 1. The robot can move freely on the concrete surface, with the microphone recording sound at the point when the hammer strikes the surface. The robot position is automatically recorded by camera. The sound and image are used for detecting defects. The proposed system has all the functions required for hammering inspection.

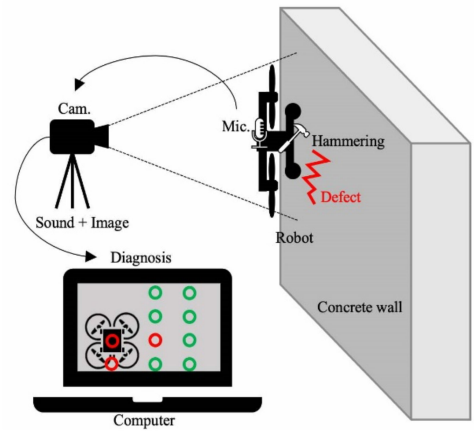

Fig. 1. Overview of hammering inspection system.

Manuscript received 28 February 2022; accepted 25 June 2022. Date of publication 15 July 2022; date of current version 29 July 2022. This letter was recommended for publication by Associate Editor T. Watanabe and Editor Y. Choi upon evaluation of the reviewers' comments. This work was supported by the JSPS KAKENHI Grant-in-Aid for scientific Research (B) under Grant JP20H02106. *(Corresponding author: Tomoyuki Yamaguchi.)*

Yuki Nishimura is with the Ph.D. Program in Empowerment Informatics, University of Tsukuba, Tsukuba 305-8577, Japan (e-mail: nishimura@ice.iit.tsukuba.ac.jp).

Shuki Takahashi is with the Master's Program in Intelligent and Mechanical Interaction Systems, University of Tsukuba, Tsukuba 305-8577, Japan (e-mail: takahashi.shuki.sp@alumni.tsukuba.ac.jp).

Hiromi Mochiyama and Tomoyuki Yamaguchi are with the Faculty of Engineering, Information and Systems, University of Tsukuba, Tsukuba 305-8577, Japan (e-mail: motiyama@iit.tsukuba.ac.jp; gucci@ice.iit.tsukuba.ac.jp).

Digital Object Identifier 10.1109/LRA.2022.3191246

For effective and accurate hammering tests, several studies on acoustic analysis methods have been conducted. Ye *et al.* [9] recorded a hammering sound dataset using a microphone and proposed a machine learning assessment method. Other studies proposed statistical analysis [10], active weak supervision analysis [11], and deep learning [12], [13]. To carry out hammering test automatically, robots must be used to strike a structure surface and collect hammering sounds. Hammering inspection systems require a special actuator mechanism which contacts the surface and generates sufficient impact force to strike surfaces. The need to maintain contact with the structure presents difficulties in controlling the robot on concrete surfaces. Based on the concept of robot-assisted human inspection, Watanabe *et al.* [14] presented a human-robot cooperative approach, in which the inspector strikes the surface with hammer and the robot analyzes the sound. However, the magnitude of the impact and repeatability of the inspection result depends on the individual human inspectors. An advantage of using robotic hammering systems is that the robot can reach areas of a concrete surface that the human inspector cannot reach. Also, the magnitude of impact by a human inspector is not constant, but robotic hammers are able to maintain a constant impact. Nakamura *et al.* [15] and Takahashi *et al.* [16] developed a tunnel inspection system. In this system, a guide frame was constructed along the tunnel surface, and a hammering mechanism moved along the guide frame. The slider-crank mechanism realized 0.5 J of impact [16]. Luk *et al.* [17] developed an automatic gondola-based robot with an impact-acoustic test device consisted of a steel sphere of diameter 12 mm and a linear solenoid actuator for pushing the steel sphere, to generate the impact force. Inoue *et al.* [18] developed a system that raised the test device using hanging wire along a vertical surface to detect the inner condition of a tile using a hammering sound [18]. Using guide frames and cables can facilitate a robust inspection, but they require a significant level of system preparation before inspection and are difficult to install in complex environments where inspectors cannot easily access.

Therefore, systems that use UAVs or mobile robots have been designed to conduct hammering tests. To install a UAV, Yang *et al.* [19] proposed a hammering mechanism with a high-pressure air tank and a cylinder, but the system has yet to be installed on actual UAV or used in practice. Salaan *et al.* [20], [21] developed a UAV with passive rotating hemispherical shells to avoid collision with structures. They installed a solenoid-based hammering device, where the solenoid will push a plunger with a hammer attached at the end, onto the UAV system. Other studies used a steel ball, a motor for a pulling a spring, and a gear and a microphone for a hammering device mounted to a UAV [22]. In Ichikawa *et al.* [22], the inspector's hammering energy was approximately 0.3 J in a usual hammering test and, to find defects at a depth approximately 100 mm from the surface, they developed a hammering device with an energy of approximately 0.3 J. Moreu *et al.* [23] proposed a UAV system with a crank mechanism actuated hammering device. Chun *et al.* [24] developed piston-type impact mechanisms, where a UAV pushes a wheel traveling mechanism mounted on its upper part against the undersurface of a bridge. Although hammering tests require contact with the structure surface under the same force, controlling a UAV to contact under same force during flight is a challenging task [25], [26]. Mobile robots, which can move on structure surfaces, can maintain a stable attitude with a constant force. Therefore, the use of climbing robots has attracted significant research attention. Li *et al.* [27] proposed a crawler-like suction cup climbing robot for impact-echo acoustic inspection. They confirmed climbing ability and inspection ability separately, but did not yet perform as an entire system because the system is too heavy to perform inspection on vertical concrete surface. Iwamoto *et al.* [28] developed a tunnel inspection robot uses multirotor thrust to push its body against tunnel surfaces, pushes the hammer solenoid to make an impact, and uses a microphone to record the impact sound. However, this robot cannot move on vertical surface, and only the striking ability is tested on composite panel. Previous hammering robots showed an ability to strike structure surfaces and record sounds, but there are no existing studies which have proposed an entire inspection system using a mobile robot, hammering device, and acoustic analysis. To develop a hammering inspection system, a light weight hammering device, which can be installed on a well-designed robot and move on surface freely, is necessary. Moreover, acoustic analysis is needed to confirm under noisy environment because the noise from robot affects the analysis. The system must demonstrate its effectiveness through experiments on concrete structures.

In this study, a novel hammering inspection system is proposed, with a hammering device consisting of a novel actuator, namely "snap-motor", and a multi-copter type mobile robot. Acoustic analysis of recorded hammering sounds is also conducted for detecting defects. The proposed hammering inspection robot system is developed to carry out all inspection procedures from moving on a surface, hammering, recording sounds and positions, to acoustic analysis. The main contributions of this study are as follows:

1) A proposed multi-copter type mobile robot can realize a stable locomotion with same constant force in same distance to the surface. A novel hammering mechanism is developed and evaluated, using a snap-motor, which can realize continuous hammering impacts despite its lightweight nature. In previous robots, attention was paid to the strength of hitting and the number of successful hits, but the influence of the hammering force of the robot was not taken into consideration. One of technical novelties of this study is that the hammering force and the stability were formulated and clarified because this relationship is important for designing hammering robots.
2) The proposed inspection system has noise suppression in an environment where the system is greatly affected by the wind noise from the multi-copters. It was difficult to classify defects when the frequency of the hammering sound features and the propeller noises were in the same band. The technical novelty here is that the timing of hammering is clarified by specifying the frequency of the propeller noise and filtering it. An accurate defect classification technology by analyzing only acoustic data including propeller noise near the hammering timing was established in this study.
3) Inspection results are obtained for a concrete structure, and these results can provide a standard benchmark for developing hammering inspection robot systems.

II. Development of Inspection System

A. Hammering Device

To install a lightweight hammering device on a climbing robot and UAV, a snap-motor was developed, which can generate a strong and quick impact with the concrete surface, using a

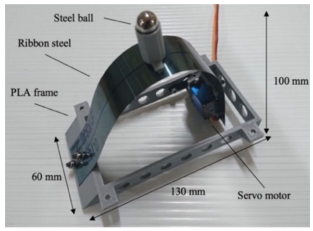

Fig. 2. Hammering device.

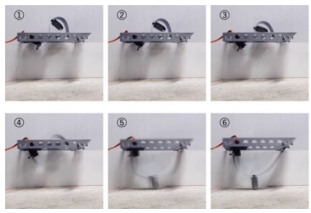

Fig. 3. Hammering sequence (60 fps).

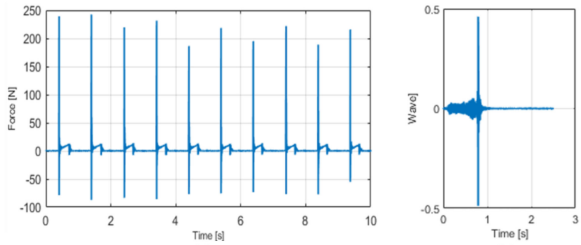

Fig. 4. Hammering force and sound. (a) Force; (b) Pure sound data.

simple mechanism. After prototyping a compact snap-through hammering mechanism, a hammering experiment was conducted using a test concrete block. In the field of biomimetic robotics, animal jumping is a significant study topic because animals jump to avoid obstacles when escaping from predators. To mimic animal jumping, an actuator which can generate quick and strong impulse forces is required. An actuator which consists of a spring metal strip, with one side is fixed and the other side rotates within an anelastic closed loop, namely closed elastica, was adopted as a focus for this study [29]. The hammering device was designed to be lightweight because multiple pieces of inspection equipment, such as a camera and hammering device, can be mounted on the robot at the same time during the inspection procedure. Usually, small actuators cannot generate enough impact, but snap-motors realize 0.3 J impact, equivalent to an inspector striking the surface.

In this study, a compact snap-through hammering mechanism was proposed, as shown in Fig. 2. The characteristic of snap-motors to generate repeated impulse forces is appropriate to strike the structure surface for hammering inspection. Moreover, the compactness is suitable for mounting on a mobile robot and UAV. The developed hammering device consisted of a steel strip, 3D printed Polylactic Acid (PLA) frame, a steel ball, and a servo motor (MG92B). The length, width, and thickness of steel strip were 200 mm, 30 mm, and 0.15 mm, respectively. The frame height, length, and width were 15 mm, 130 mm, and 60 mm, respectively. The servo motor was controlled with a microcontroller. The steel ball diameter was 10 mm, and the mass was 4 g. The total mass of the hammer part, including the hammer head, ribbon steel, and the screws was 17 g. The total weight of the device was 60 g. Where, in the preliminary experiment, we confirmed that the device can hit the object more than 20000 times with 1 Hz frequency.

Fig. 3 shows sequence of strikes by the developed hammering device. The video was taken with 60 fps, so each picture in Fig. 3 represents motion in 1/60 s intervals. In frames 1 to 3, the servo motor moved and the steel strip slowly bended. From frames 4 to 5, after the servo motor moved to a certain angle, the deformed steel strip stretched quickly. The hammer head moved approximately 0.1 m in 1/60 s, so the velocity of striking was 6 m/s. Then, the hammer struck the concrete in frame 6. After hammering, the servo motor moved back to its initial position. Therefore, the device was able to hammer concrete continuously. The kinetic energy of hammering was calculated using (1), where *KE* is the energy, *m* is the mass of hammer part, and *v* is the velocity of striking.

$$KE = \frac{1}{2}mv^2 \tag{1}$$

From substituting the experimental parameters, *m* is 0.017 kg and *v* is 6 m/s from the experiment shown in Fig. 3. The hammering energy of the device was approximately 0.306 J. In Ichikawa *et al.* [22], the energy of a human inspector hammering assumed to be approximately 0.3 J to find defects at a depth of approximately 100 mm from the surface. Therefore, the developed device is able to generate and apply the same energy to structures as a human inspector hammering during manual inspection procedures.

The hammering force of the developed device was measured to evaluate whether the device can hit the surface with a constant force in each impact. 10 impacts were measured with a loadcell set on the hitting point of hammering device. The sampling rate of the loadcell was 16 kHz. The frequency of hammering was 1 Hz. As shown in Fig. 4(a), impulses were observed when the hammer hit the loadcell. From the result, with the developed snap-motor hammering device, even with a small mass, the device can generate a constant force. The average force was 215.9 N, and the standard deviation was $\pm$19.97 N. The developed hammering device can hit the structure surface continuously once per s with a distribution of $\pm 10\%$ or less. To check an influence of a small force observed after the hammering force, the pure sound data when hit only once was shown in Fig. 4(b). As only one peak can be confirmed, there is no influence on double hammering. This is initial force from hammering device to wall because the hammer head was placed about 5 mm aside to the structure side so that the hammer contacts the surface with enough power.

B. Inspection Robot

In this study, a mobile robot with a multi-copter was developed. Mobile robots using multi-copter thrust forces have been proposed in several studies [30]–[35]. The robot uses the thrust force from the multi-copter to push its body against the surface, therefore, the robot can maintain its attitude on a structure surface. This type of robot has no limitations for surface shapes and materials, compared to suction-type or magnetic-type climbing robots. Moreover, multi-copter type mobile robot can maintain a constant contact force and distance from the surface to perch on the surface; therefore, the hammering stroke distance and hammering force will be maintained in small deviation.

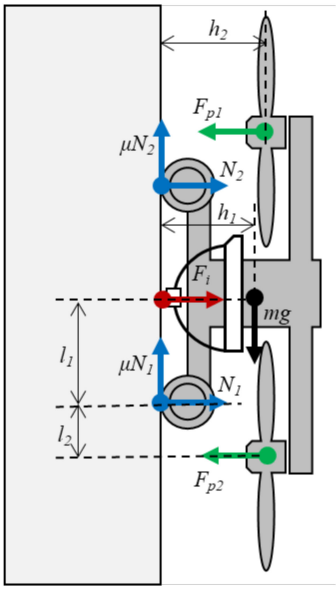

Fig. 5. Force diagram of proposed robot.

There are two stable conditions for a robot on vertical surface; the friction force and the moment [36]. The force diagram of the proposed robot is shown in Fig. 5. F_{p1} is the thrust force from the propellers on the upper side, and F_{p2} is the thrust force from the propellers on the lower side. N_1 and N_2 are the normal forces, as reaction forces of F_{p1} and F_{p2}, respectively. μ is the friction coefficient, so μN is the friction force, m is the mass of the robot, and g is the gravitational acceleration. h_1 and h_2 are the height to the center of mass and the propellers from a surface, respectively, and l_1 and l_2 are the length to the center of mass and the propellers from a wheel, respectively. The stable condition on the friction force is written as Eq. (2), and the stable condition on the moment applied to the robot is written as Eq. (3). The positive moment is counterclockwise, and the center of moment is the contact point of the lower wheel of the robot and the vertical surface.

$$\mu(F_{p1} + F_{p2}) > mg \tag{2}$$

$$-F_{p1}l_2 - mgh_1 - 2N_2l_2 + F_{p2}(2l_1 + l_2) \geq 0 \tag{3}$$

In the case of a hammering test robot, the robot applies force to the surface. Therefore, the reaction force of this impact must be included in the stable condition. When the device is installed at the center of a robot and F_i is average hammering force per unit time, the stable conditions of friction and moment are written as (4) and (5), respectively. Equations. (4) and (5) are modifications of Eqs. (2) and (3).

$$\mu(F_{p1} + F_{p2} - F_i) > mg \tag{4}$$

$$-F_{p1}l_2 - mgh_1 - 2N_2l_2 + F_{p2}(2l_1 + l_2) - F_il_1 \geq 0 \tag{5}$$

From Eq. (5), a large negative moment makes the robot unstable. While the mass of the robot cannot be changed, h_1 in Fig. 5 is the only parameter to reduce the effect of the moment. Therefore, the position of the battery was set at a lower position in the developed robot. To reduce a loss of friction force when the robot turns on the structure surface, a steering wheel with a servo motor was installed to realize smoother turning on a surface. Thus, from revised Eq. (4), the relationship between the average of the hammering force and the thrust force can be clarified. Also, from Eq. (5), it was possible to clarify that the average of the hammering force and its mounting position are important.

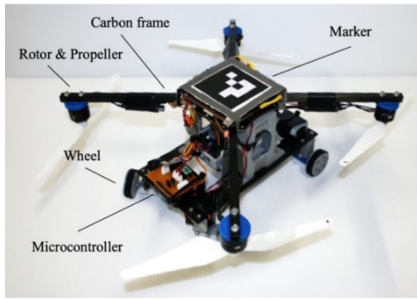

Fig. 6. Overview of the developed robot.

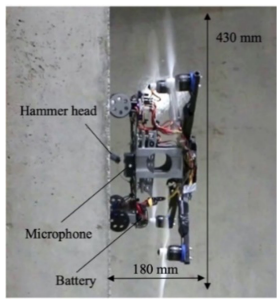

Fig. 7. Side view of the robot on the wall.

An overview and side view of the developed robot are shown in Figs. 6 and 7, respectively. The hammering device was mounted on the center of robot. The robot body consisted of a carbon pipe as arms to support the propeller, a 3D printed part of PLA as a frame, and Carbon Fiber-reinforced polymers (CFRP) board as the robot base. The robot had four rotors (E310 2312 by DJI) with 9450 propellers, and four 12V DC motors for the wheel (1000:1 HPCB 12V by Pololu). For steering the robot, two servo motors (SG90 by TowerPro) were installed above 12V DC motors. The Li-po battery (11.1V, 1800 mAh) supplied power to all actuators and a microcontroller. The length, width, and height including propellers were approximately 430 mm, 430 mm, and 180 mm, respectively. The mass was 1.17 kg, including the developed hammering device and battery. The robot speed is 4.4 m/min. The continuous operating time of the battery used in the proposed robot is 10 minutes. The operation time depends on battery size, however, our robot can also operate with power supply cable. At the place where cable can reach, the system uses cable and realizes a long-time inspection. As shown in Fig. 7, the thrust force pushed the robot onto the surface to maintain a stable attitude on the structure. In case where the hammer head is placed on the same level as the surface level, the hammer will miss striking the structure. Therefore, the hammer head was placed about 5 mm aside to the structure side so that the hammer contacts the surface with enough power. The microphone was installed underneath the robot near the hammering point. The robot neither fall down and slip down on surface from Eqs. (4) and (5). The thrust force of four propellers was 23.52 N which means F_{p1} and F_{p2} are 11.76 N in upper side and downside. h_1 is 50 mm, l_1 is 105 mm, and l_2 is 50 mm. Rubber and concrete coefficient of friction is approximately 0.72. *Fi* was measured from Fig. 4(a), and the average of 10 hit data was calculated, which was 2.48 N. The left side of Eq. (4) is 15.15 N and the

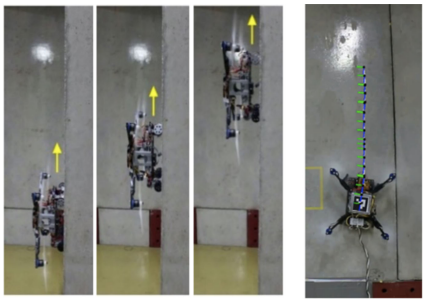

Fig. 8. Climbing experiment of developed robot.

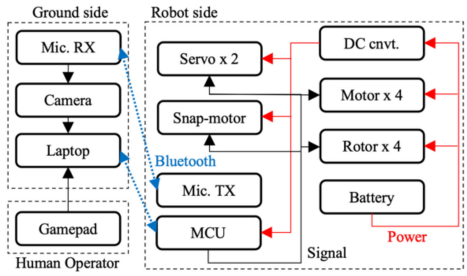

Fig. 9. Block diagram of signal and power flow.

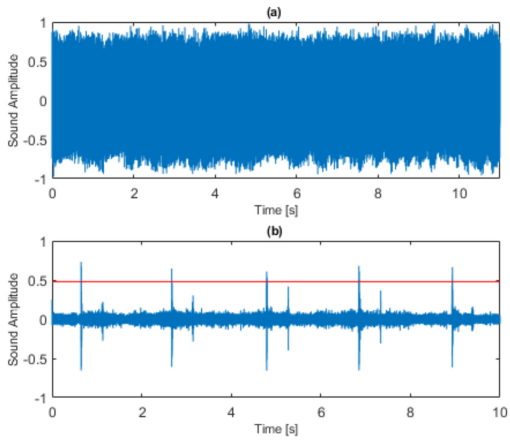

Fig. 10. (a) Original sound and (b) filtered sound.

right side is 11.47 N, which satisfies Eq. (4). The same can be said for Eq. (5).

To confirm that the proposed mobile robot design realized the climbing motion on a vertical concrete surface, a fundamental experiment was conducted. This experiment determined whether the developed robot was able to climb the vertical surface while hammering the structure. First, the robot was set on the lower surface of the concrete structure and then moved up the surface. The robot movements on the surface are shown in Fig. 8(left). Each image represents the image captured in intervals of 5 s. It was observed that the robot can move up the vertical surface with a stable attitude with the hammering device without falling and the mounted hammering device can appropriately strike the surface. Fig. 8(right) shows basic performance for straightness and posture stability (vertical: blue, horizontal: green) while hitting the wall with a hammer. Five experiments were conducted in which the robot moved 50 cm while moving and hitting vertically, and the error of 3.1 cm was horizontal on average. In each experiment, the robot hit about 10 times with a movement of 50 cm, so the error caused by hitting once was 3.7 mm, and the standard deviation was 1.1. The absolute angle error per hit was 0.6 deg, and its standard deviation was 0.4. This angle error that occurred is considered to be the effect of the slight asymmetry of the developed robot. Since the diameter of hammer head was 10mm, the error within that range is acceptable.

C. Measurement of Hammering Positions and Sounds

The developed hammering device's ability to strike a concrete structure with the necessary energy to inspect concrete health was confirmed. Furthermore, the developed robot's ability for locomotion on a concrete surface and to move to the desired point to hammer was verified. For finding the hammering position on a structure, an Augmented Reality (AR) marker [37], [38] was used for localization. The AR marker was placed on top of the developed robot. A PC and a camera were prepared on the ground side. Then, the camera captured the developed robot on the structure surface. From the captured image, the robot position was calculated.

The system's process for detecting the timing of hammering is explained here. The inspection system should record the hammering sounds as well as the hammering position. For recording sounds, a Bluetooth microphone (Wireless GO by RODE) was used, which can transfer high quality sound to the ground side. The microphone was equipped underneath of the robot base to record hammering sounds in close proximity to the contact point of the hammer head and the structure. Also, this position is effective to reduce noise from the propeller rotation for acoustic analysis. While the position of the robot was localized by the AR marker, the video and sound from the microphone were synchronized. A block diagram of the signal flow is shown in Fig. 9. A certain value was set as the threshold of the wave amplitude for recording sounds. If the robot hit the structure with a hammering device, the wave amplitude crossed the threshold, and the system recognized when hammering occurred.

However, the recorded sounds contained wind noises from rotating propellers of the robot. Due to these wind noises, the time when hammering occurred was difficult to determine. Therefore, a high pass filter was applied to denoise. The cut-off frequency was 10 kHz, and the amplitude threshold was set. When the amplitude crossed this threshold, the system detected that the hammering occurred. The original signal and denoised signal of the first five hammering attempts from the first trial are shown in Fig. 10. In the denoised signal, the small peak appeared after the hammering peak. These peaks were generated from the sound made when ribbon steel reverted back to its initial position.

In Fig. 11, the robot path and hitting points are shown when the robot moved along the surface while hitting the concrete structure. The robot could move freely on the surface and make strikes. The robot path, estimated by the AR marker, is shown with the white line, and the hitting points, estimated with the threshold, are shown as white dots.

D. Acoustic Analysis

Acoustic analysis for the hammering inspection robot must be designed to function even under high wind noise from multicopter. Here, the dataset produced throughout the experiment is introduced. With a high pass filter and the threshold, the timing of hammering can be determined. This timing was used to cut

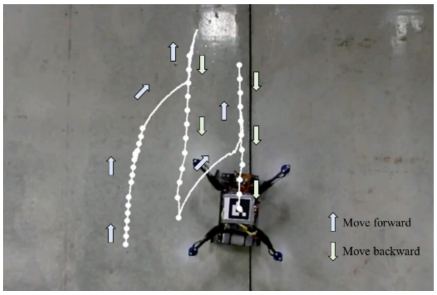

Fig. 11. Estimation of robot path and hitting point.

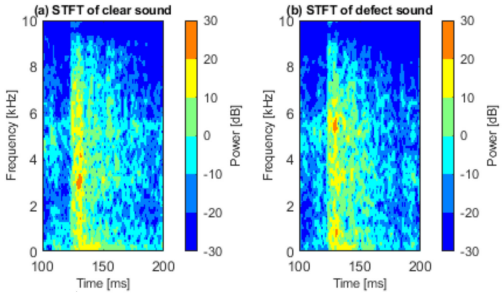

Fig. 12. STFT without noises. (a) clear sound with a peak at 3 kHz; (b) defect sound with a peak at 5.5 kHz.

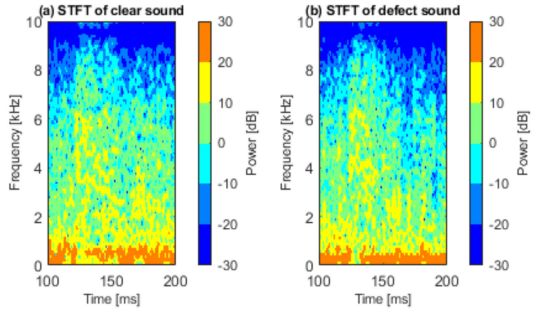

Fig. 13. STFT of hammering sounds with noise from multi-copter. (a) result of clear sound; (b) result of defect sound.

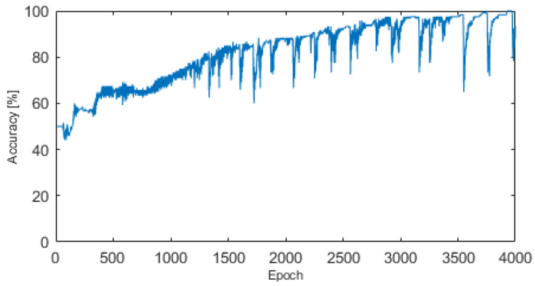

Fig. 14. Training accuracy vs. epochs (1-4000).

the original sound file into single hammering sound data with a duration of 0.5 s. Each data consisted of 24000 sampling points, in which 25% (6000 sampling points) were before and 75% (18000 sampling points) were after crossing the peak threshold. The original sound file was used to create a sound dataset because the denoised hammering sound lost some features on the structural characteristics.

To determine the sound characteristics of the experiment concrete structure, hammering sounds were recorded using the developed system on a clear area and a defected area. To produce sounds without the propeller noise, the robot was manually held against a surface while a hammering device on the robot struck the structure. The sounds were recorded by a microphone with a 48 kHz sampling rate. Spectrum analysis was applied to the recorded sound dataset to analyze the sounds. Fig. 12 shows the characteristic results of Short-time Fourier Transform (STFT) on clear sound and defected sound. Hammering occurred at approximately 130 ms. The clear sound peaked around 2.5 kHz. Compared to clear sounds, the defect sound had a peak at a frequency range of 5-6 kHz. From experience, the defected concrete is known to generate higher frequency sounds compared to normal concrete. The results confirmed that the defected area produced higher frequency sounds. In contrast, the hammering sounds recorded from this system contain drone noise which causes a wide frequency range. The STFT results of noised sounds are shown in Fig. 13, where it is difficult to distinguish the characteristics of hammering sounds. Also, the power spectral changes depending on the concrete structure and environment. Therefore, the use of deep learning to automate hammering inspection for complicated concrete structures is a commonly research focus [12], [13].

In this study, a simple two-class classification was used to separate the sounds labeled clear and the sounds labeled defect. First, a training dataset was produced of clear sounds and defected sounds when the developed robot perches on the surface by the propellers' force and the hammering device hits the structure. A total of 120 hammering sounds (60 clear sounds and 60 defect sounds) were collected for training. For classification, a fully connected layer based on the MATLAB deep learning toolbox was built [39]. The final model can separate the training dataset with 100% accuracy, even if the sounds contain strong noises. The validation result is explained in following section, because the corrected sounds from actual experiment were used as the validation data to evaluate the classification (Fig. 14). For plotting the experimental results, the best validation accuracy scored models were selected from the models that achieved 100% accuracy in the training data.

III. Experiment and Results

In this section, the experiment used to verify the developed hammering inspection system is described. During the experiment, the robot performed stable movements on a surface of concrete structure. A two-class classification was applied to distinguish defected unhealthy sounds from clear and healthy sounds. First, the experimental environment is explained. Then, the experiment used to evaluate the inspection capability of the developed system is outlined.

A. Experiment Environment

Two concrete structures, *Test 1* and *Test 2*, were used for experiments of the robot with the hammering device. *Test 1* had a stage, three concrete structures, and a ceiling. All parts were fastened with bolts. The height, including the steel stage, was 1980 mm, the width was 2280 mm, and the depth of the concrete structure was 150 mm. The inside of the concrete, a 200 mm square plastic plate, was embedded at a 30 mm depth from the surface to simulate a defect inside a concrete structure (red area). The plastic plate was located 900 mm from the left side, and 1080 mm from the top of the structure as shown with the red square. *Test 2* is concrete with artificial peelings surface made by

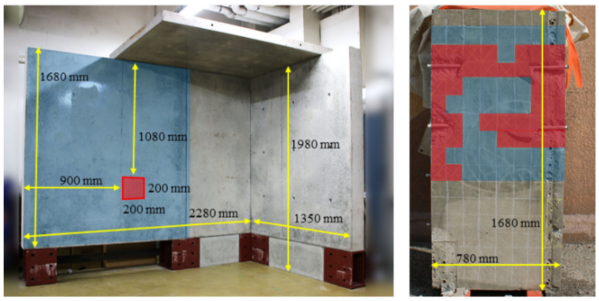

Fig. 15. Experiment structures *Test 1*(left), *Test 2*(right).

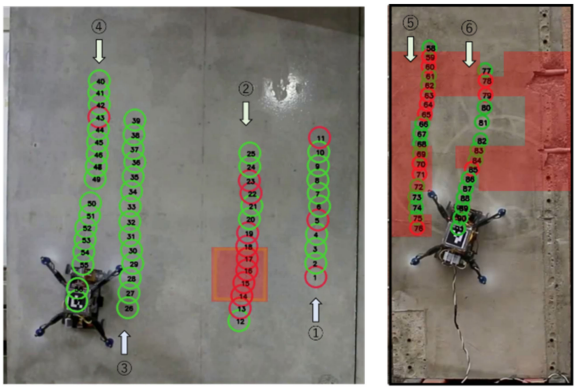

(a) (b)

Fig. 16. Hammering results. (a) *Test 1*; (b) *Test 2*.

pipes filled with expansion agent [40]. The height was 1680 mm, the width was 780 mm, and the depth was 150mm. The depth is shared with *Test 1* because hammering sounds are largely affected by concrete depth. The expert inspector performed the hammering test and marked the correct defective area (red area). It was assumed that these structures simulate the complex real environment as sufficiently as the test structure for hammering test studies.

B. Experiment Results

The developed robot travelled on the experimental concrete structure while hammering. A camera was set 3 m from the surface. The hammering sounds by the developed robot on the surface were recorded with the mounted microphone with a 48 kHz sampling rate. Based on the captured video and sound, the travel path of the robot was calculated with an AR maker on top of the robot and the hammering timing was calculated with the amplitude threshold. Several trials were conducted to collect data on the structure, shown as the blue area in Fig. 15.

While the developed robot was moving on the surface, the hammering device struck the structure, and the sounds were recorded. The recorded sounds were classified as defected or clear. The results are plotted in Fig. 16 as hitting point circles with timings. In *Test 1*, the total number of recorded hammering sounds was 57. Amongst those, 6 sounds were collected when the AR marker overlapped on the defected area and 51 sounds were collected by hammering the non-defected area. The collected sounds were classified into defect or clear labels with a trained classifier. The hitting timing and points with classified results are plotted on the captured video image shown in Fig. 16. The numbered timings is a sequence of hammerings.

TABLE I
CLASSIFICATION RESULTS

	Spectral Analysis			Proposed		
	Test	Test	Total	Test	Test	Total
Total hit	57	36	93	57	36	93
True Positive	0	0	0	6	12	18
False Positive	0	0	0	7	2	9
True Negative	51	16	67	44	14	58
False Negative	6	20	26	0	8	8
Accuracy (%)	89.5	55.6	72.0	87.7	72.2	81.7
Recall	0.0	0.0	0.0	1.0	0.6	0.69
Precision	-	-	-	0.46	0.86	0.67

The classification results are shown as circles. The color of the circle represents the label; red circles are defected and green circles are clear. Table I shows the prediction results of the classification. We compared the proposed method and the method using spectral analysis [22].

C. Discussion

Throughout the experiment, it was confirmed that the developed robot satisfies the abilities which are required for a hammering inspection robot system. The developed multi-copter type mobile robot showed stable movement on the surface even under the force of the hammering device striking the structure. The hammering sounds were collected, and the locations were captured for hammering points. Therefore, the defect can be detected in the concrete structure by analyzing the relationship between sounds and positions.

In environments where noise occurs, such as using a UAV or a mobile robot, the sound characteristics are difficult to be determined by the spectral analysis using STFT or Fast Fourier Transform (FFT) from Table I. Total *Accuracy* was 72.0%, and *Recall* and *Precision* were 0.0 and -, respectively. This is because all hammering sound data is predicted as clear, and no defects have been detected. On the other hand, the total *Accuracy* is 81.7% in the proposed method. *Recall* and *Precision* were 0.69 and 0.67, respectively. This means that the proposed system recorded the characteristics of defect sounds by hammering with the developed device. Further, the deep-learning-based classification is effective for the hammering test mobile robot system. *Recall* was 1.0 for the *Test 1* concrete used for the trained model. In the case of *Test 2*, it is scored 0.69 as *Recall*, however, the *Accuracy* was 72.2%. The proposed method quantitatively showed robustness and the proposed inspection robot can be applied even on different walls in the presence of propeller noise.

For practical usage, the condition of the concrete can be evaluated by hammering the surface with a high density once the hammering sounds are predicted as a defect. The actual defect can be predicted using the relationship with surrounding results. In this case, the hammering sounds at numbers 13 to 19 were predicted as a defect, and the actual conditions around this series of sounds were also defects. At numbers 5 and 45, the sounds were predicted as defects, but the surroundings were predicted as clear. Therefore, these points can be estimated as clear by inspecting as an area rather than as points. Collecting sound data in series by smooth and continuously hammering while moving on surfaces is a strength of the developed robot system. Therefore, by hammering densely, this system can be used in real concrete health monitoring.

IV. Conclusion

In this paper, a hammering inspection system for concrete structures was proposed. An inspection robot installed with a hammering device with a snap-motor was developed, which with a multi-copter can maintain the same distance from the wall. The hammering device generated impact sounds, which were distinguished as clear sound or defect sound experimentally. It was confirmed that the developed system has an ability to conduct hammering tests under noisy environment. The inspection experiment on the real concrete structure showed that the proposed system was able to detect internal concrete defects with total *Accuracy* of 81.7%.

Based on the outcomes of this study, future work should involve detailed analysis of the hammering sounds to improve accuracy of defect detection. Moreover, future research will focus on collecting broader experiment results on real structures such as bridges and buildings, which include ceiling or curved surface, under different environment to evaluate utility of the proposed hammering inspection system.

References

[1] S. Tadokoro et al., "The world robot summit disaster robotics category – achievements of the 2018 preliminary competition," *Adv. Robot.*, vol. 33, no. 17, pp. 854–875, 2019.

[2] H. Fujii, A. Yamashita, and H. Asama, "Defect detection with estimation of material condition using ensemble learning for hammering test," in *Proc. IEEE Int. Conf. Robot. Automat.*, 2016, pp. 3847–3854.

[3] C. Koch, K. Georgieva, V. Kasireddy, B. Akinci, and P. Fieguth, "A review on computer vision based defect detection and condition assessment of concrete and asphalt civil infrastructure," *Adv. Eng. Inform.*, vol. 29, no. 2, pp. 196–210, 2015.

[4] P. Sekhar and R. S. Bhooshan, "Duct fan based wall climbing robot for concrete surface crack inspection," in *Proc. Annu. IEEE India Conf.*, 2014, pp. 1–6.

[5] L. Yang, Y. Chang, B. Jiang, and J. Xiao, "Visual SHM for concrete infrastructure using a Wall-climbing robot," in *Proc. 9th Int. Conf. Struct. Health Monit. Intell. Infrastructure*, 2019, pp. 896–901.

[6] J. P. Z. De Paz, E. C. Castañeda, X. Y. S. Castro, and S. M. R. Jiménez, "Crack detection by a climbing robot using image analysis," in *Proc. 23rd Int. Conf. Electron., Commun. Comput.*, 2013, pp. 87–91.

[7] H. Kim, J. Lee, E. Ahn, S. Cho, M. Shin, and S.-H. Sim, "Concrete crack identification using a UAV incorporating hybrid image processing," *Sensors*, vol. 17, no. 9, 2017, Art. no. 2052.

[8] H. Yu, W. Yang, H. Zhang, and W. He, "A UAV-based crack inspection system for concrete bridge monitoring," in *Proc. Int. Geosci. Remote Sens. Symp.*, 2017, pp. 3305–3308.

[9] J. Ye, T. Kobayashi, M. Iwata, H. Tsuda, and M. Murakawa, "Computerized hammer sounding interpretation for concrete assessment with online machine learning," *Sensors*, vol. 18, no. 3, 2018, Art. no. 833.

[10] K. Hagiwara, A. Yasojima, T. Shibuya, and T. Yamaguchi, "Real-time defect detection method without training data for hammering test support system," in *Proc. Int. Symp. System Integration*, 2019, pp. 205–209.

[11] J. Y. L. Kasahara, A. Yamashita, and H. Asama, "Acoustic inspection of concrete structures using active weak supervision and visual information," *Sensors*, vol. 20, no. 3, 2020, Art. no. 629.

[12] Y.-F. Shih, Y.-R. Wang, S.-S. Wei, and C.-W. Chen, "Improving non-destructive test results using artificial neural networks," *Int. J. Mach. Learn. Comput.*, vol. 5, pp. 480–483, 2015.

[13] T. Fukumura, H. Aratame, A. Ito, M. Koike, K. Hibino, and Y. Kawamura, "A study on hammering test using deep learning," in *Proc. IEEE 15th Int. Conf. System Syst. Eng.*, 2020, pp. 261–264.

[14] A. Watanabe, J. Even, L. Y. Morales, and C. Ishi, "Robot-assisted acoustic inspection of infrastructures – Cooperative hammer sounding inspection," in *Proc. Int. Conf. Intell. Robots Syst.*, 2015, pp. 5942–5947.

[15] S. Nakamura et al., "Inspection test of a tunnel with an inspection vehicle for tunnel lining concrete," *J. Robot. Mechatronics*, vol. 31, no. 6, pp. 762–771, 2019.

[16] Y. Takahashi, S. Nakamura, Y. Ogawa, and T. Satoh, "Velocity control mechanism of the under-actuated hammering robot for gravity compensation," in *Proc. Int. Symp. Automat. Robot. Construction*, 2017, vol. 34, pp. 1–6.

[17] B. L. Luk, K. P. Liu, Z. D. Jiang, and F. Tong, "Robotic impact-acoustics system for tile-wall bonding integrity inspection," *Mechatronics*, vol. 19, no. 8, pp. 1251–1260, 2009.

[18] F. Inoue, S. Doi, T. Ishizaki, Y. Ikeda, and Y. Ohta, "Study on automated inspection robot and quantitative detection of outer tile wall exfoliation by wavelet analysis," in *Proc. Int. Conf. Control, Automat. Syst.*, 2010, pp. 994–999.

[19] Y. Yang, A. Cattaneo, and D. Mascareñas, "Potential structural health monitoring tools to mitigate corruption in the construction industry associated with rapid urbanization," in *Proc. 3rd Annu. Int. Conf. Sustain. Develop. Pract. Implementing SDGs: Getting Started*, 2015, pp. 1–13.

[20] C. J. Salaan, K. Tadakuma, Y. Okada, K. Ohno, and S. Tadokoro, "UAV with two passive rotating hemispherical shells and horizontal rotor for hammering inspection of infrastructure," in *Proc. IEEE/SICE Int. Symp. System Integration*, 2017, pp. 769–774.

[21] C. J. Salaan, K. Tadakuma, Y. Okada, Y. Sakai, K. Ohno, and S. Tadokoro, "Development and experimental validation of aerial vehicle with passive rotating shell on each rotor," *IEEE Robot. Automat. Lett.*, vol. 4, no. 3, pp. 2568–2575, Jul. 2019.

[22] A. Ichikawa et al., "UAV with manipulator for bridge inspection — Hammering system for mounting to UAV," in *Proc. IEEE/SICE Int. Symp. System Integration*, 2017, pp. 775–780.

[23] F. Moreu, E. Ayorinde, J. Mason, C. Farrar, and D. Mascarenas, "Remote railroad bridge structural tap testing using aerial robots," *Int. J. Intell. Robot. Appl.*, vol. 2, pp. 67–80, 2018.

[24] P.-J. Chun et al., "Utilization of unmanned aerial vehicle, artificial intelligence, and remote measurement technology for bridge inspections," *J. Robot. Mechatronics*, vol. 32, no. 6, pp. 1244–1258, 2020.

[25] T. Ikeda et al., "Wall contact by octo-rotor UAV with one DoF manipulator for bridge inspection," in *Proc. IEEE/RSJ Int. Conf. Intell. Robots Syst.*, 2017, pp. 5122–5127.

[26] T. Ikeda et al., "Stable impact and contact force control by UAV for inspection of floor slab of bridge," *Adv. Robot.*, vol. 32, no. 19, pp. 1061–1076, 2018.

[27] B. Li, K. Ushiroda, L. Yang, Q. Song, and J. Xiao, "Wall-climbing robot for non-destructive evaluation using impact-echo and metric learning SVM," *Int. J. Intell. Robot. Appl.*, vol. 1, pp. 255–270, 2017.

[28] T. Iwamoto, T. Enaka, and K. Tada, "Development of testing machine for tunnel inspection using multi-rotor UAV," *J. Phys.: Conf. Ser.*, vol. 842, no. 1, 2017, Art. no. 012068.

[29] H. Mochiyama, "Model validation of discretized spatial closed elastica," in *Proc. Int. Conf. Intell. Robots Syst.*, 2016, pp. 5216–5223.

[30] J. Shin, D. Kim, J. Kim, and H. Myung, "Micro aerial vehicle type wall-climbing robot mechanism," in *Proc. IEEE RO-MAN*, 2013, pp. 722–725.

[31] P. Beardsley et al., "VertiGo – A wall-climbing robot including ground-wall transition," 2015. [Online]. Available: https://disneyresearch.com/publication/vertigo/

[32] W. C. Myeong, K. Y. Jung, S. W. Jung, Y. H. Jung, and H. Myung, "Drone-type wall-climbing robot platform for structural health monitoring," in *Proc. Int. Conf. Adv. Exp. Struct. Eng.*, 2015, pp. 286–389.

[33] K. Ioi, Y. Shimizu, and M. Kimura, "Experiments and simulations of wall running and transferring of a climbing robot," in *Proc. Int. Symp. Innovations Intell. Syst. Appl.*, 2015, pp. 1–7.

[34] M. Alkalla, M. Fanni, A. Mohamed, and S. Hashimoto, "Tele-operated propeller-type climbing robot for inspection of petrochemical vessels," *Ind. Robot*, vol. 44, no. 2, pp. 166–177, 2017.

[35] Y. Nishimura and T. Yamaguchi, "Development of a steep slope mobile robot with propulsion adhesion," in *Proc. Int. Conf. Intell. Robots Syst.*, 2020, pp. 2592–2599.

[36] H. Huang et al., "Design and performance analysis of a tracked wall-climbing robot for ship inspection in shipbuilding," *Ocean Eng.*, vol. 131, pp. 224–230, 2017.

[37] F. J. Romero-Ramirez, R. Muñoz-Salinas, and R. Medina-Carnicer, "Speeded up detection of squared fiducial markers," *Image Vis. Comput.*, vol. 76, pp. 38–47, 2018.

[38] R. Muñoz Salinas, F. J. Madrid-Cuevas, and R. Medina-Carnicer, "Generation of fiducial marker dictionaries using mixed integer linear programming," *Pattern Recognit.*, vol. 51, pp. 481–491, 2016.

[39] MathWorks, Inc, Classify Sound Using Deep Learning, Accessed: Dec. 9, 2021. [Online]. Available: https://mathworks.com/help/audio/gs/classify-sound-using-deep-learning.html

[40] A. S. Syll et al., "Bond strength degradation in concrete cracked by expansion agent filled pipes," *Struct. Concrete: J. FIB*, vol. 22, no. 5, pp. 3156–3172, 2021.